Electronic Supplementary Material (ESI) for Nanoscale.

Supporting Information

Exquisite Design of Porous Carbon Microtubule-Scaffolding Hierarchical In_2O_3-$ZnIn_2S_4$ Heterostructures toward Efficiently Photocatalytic Conversion of CO_2 into CO

Wa Gao,[a] Lu Wang,[a] Chao Gao,[e] Jinqiu Liu,[a] Yong Yang,[f] Liuqing Yang,*[a] Qing Shen,[d] Congping Wu,[a,c] Yong Zhou, *[a,b,c] and Zhigang Zou[a,b,c]

[a] *National Laboratory of Solid State Microstructures,Collaborative Innovation Center of Advanced Microstructures, School of Physics, Nanjing University, Nanjing 210093, P. R. China.* E-mail: zhouyong1999@nju.edu.cn

[b] *Key Laboratory for Nano Technology, Nanjing University, Nanjing 210093, P. R. China.* E-mail: liuqingyang@nju.edu.cn

[c] *Kunshan Sunlaite New Energy Co., LTd, Kunshan Innovation Institute of Nanjing University, Kunshan, Jiangsu 215347, P. R. China.*

[d] *Faculty of Informatics and Engineering, the University of Electro-Communications, Tokyo 182-8585, Japan.*

[e] *Univ Sci & Technol China, Hefei Natl Lab Phys Sci Microscale, iChEM Collaborat Innovat Ctr Chem Energy Mat, Sch Chem & Mat Sci,Natl Synchrotron Radiat Lab, Hefei 230026, Anhui, Peoples R China.*

[f] *Key Laboratory of Soft Chemistry and Functional Materials (MOE), Nanjing University of Science and Technology, Nanjing 210094, P. R. China.*

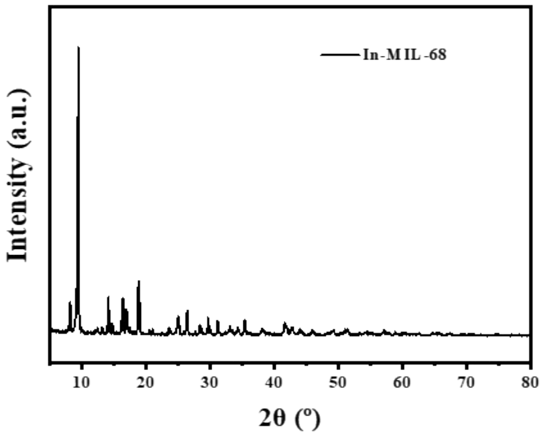

Figure S1. XRD pattern of In-MIL-68.

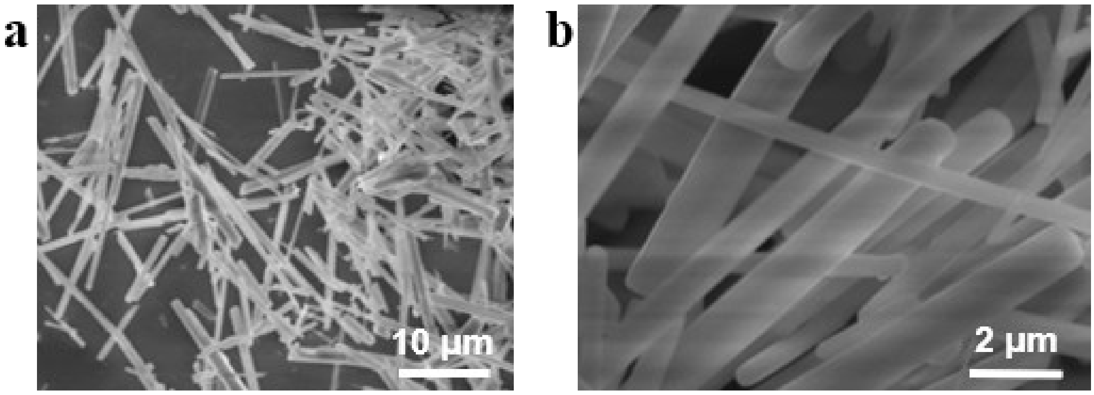

Figure S2. (a, b) FE-SEM images of In-MIL-68.

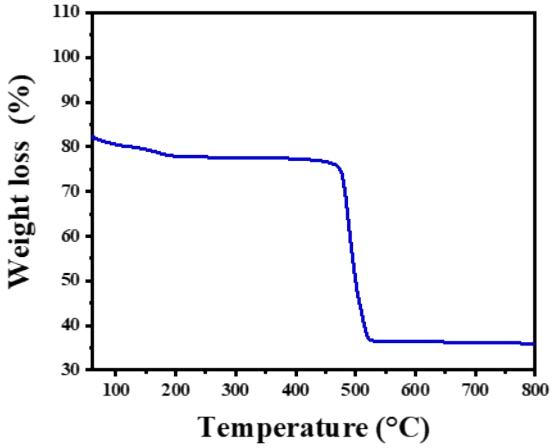

Figure S3. TGA curve of In-MIL-68 in air atmosphere with a heating rate of 5 °C min^{-1}.

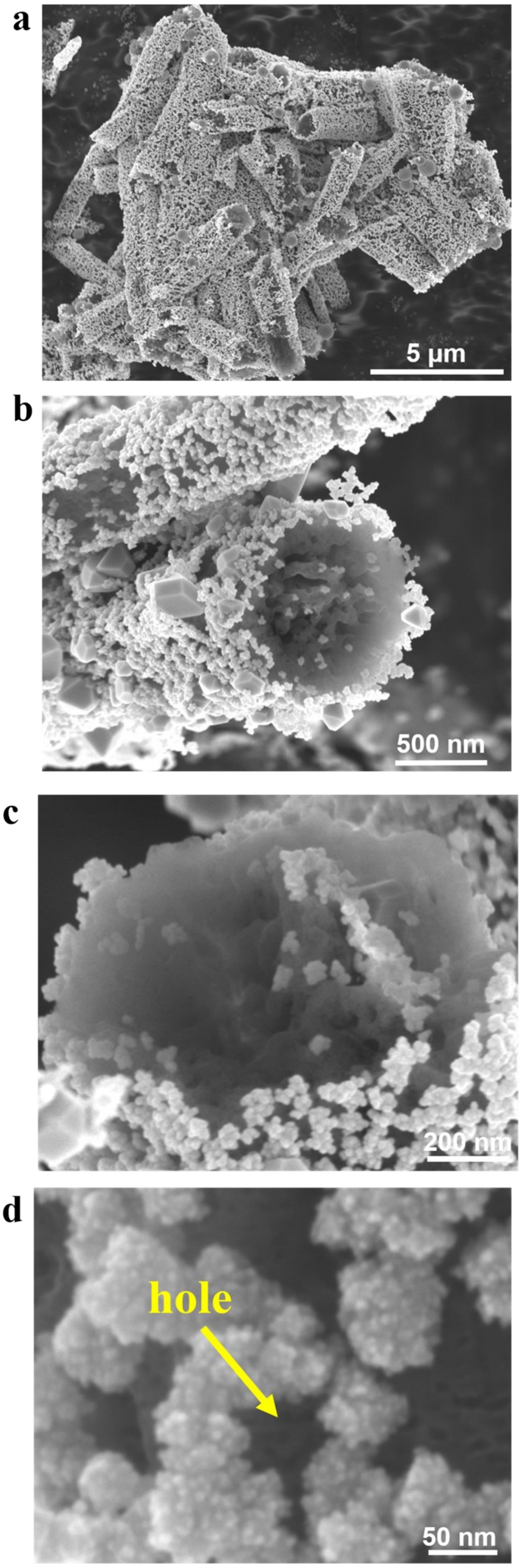

Figure S4. (a-d) SEM images of PCMT@In_2O_3 with well-defined open ends after calcination.

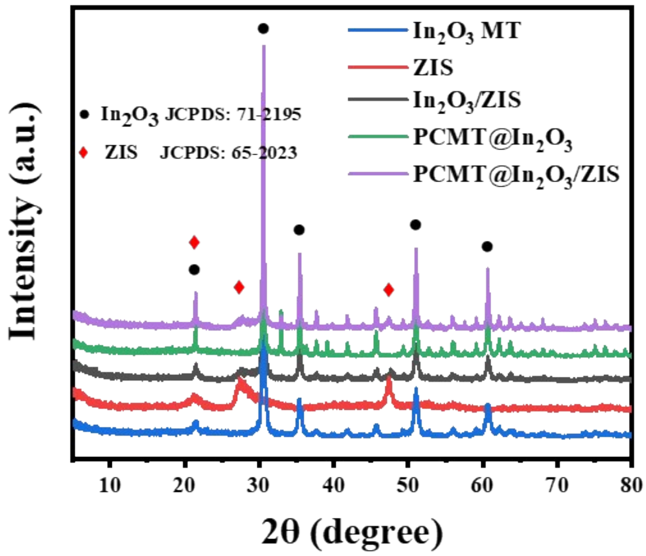

Figure S5. The corresponding XRD patterns of different samples.

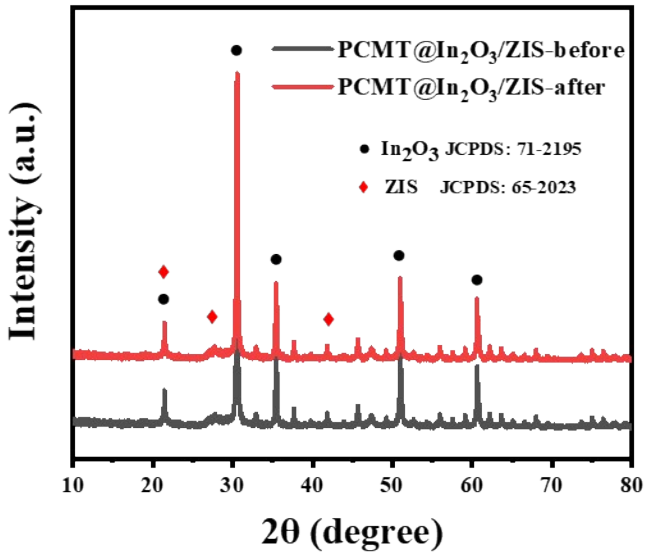

Figure S6. The corresponding XRD patterns of PCMT@In_2O_3/ZIS before and after photocatalytic CO_2 reduction test.

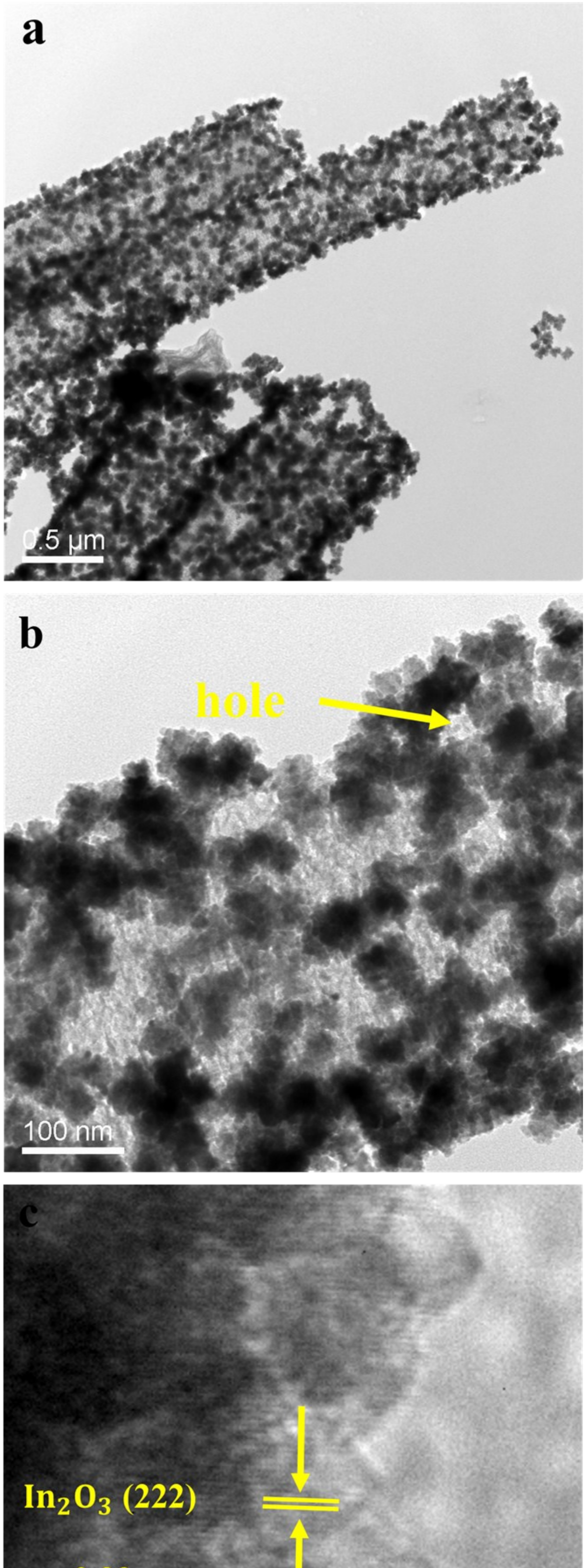

Figure S7. (a, b, c) TEM and (d) HRTEM image of PCMT@In_2O_3.

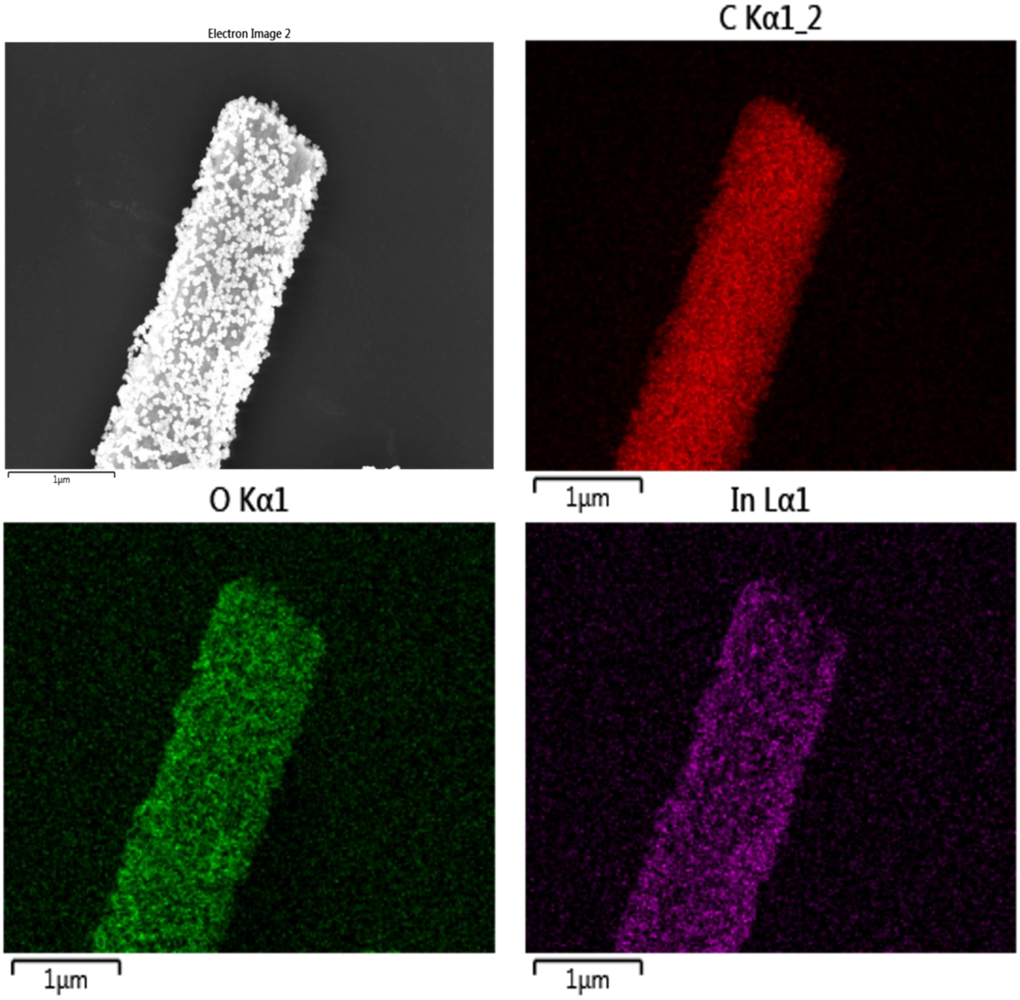

Figure S8. STEM-EDX elemental mapping for PCMT@In_2O_3

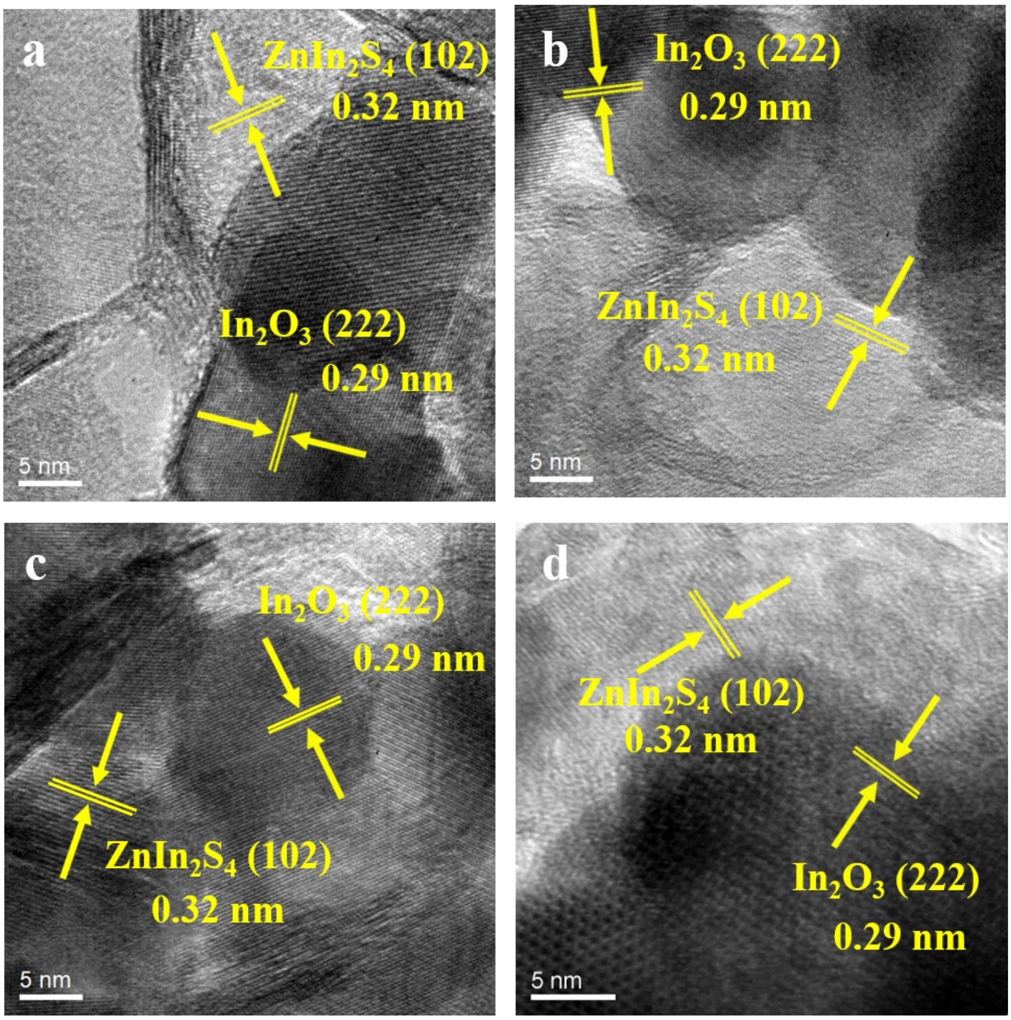

Figure S9. More HRTEM observation of the presence for PCMT@In_2O_3/ZIS.

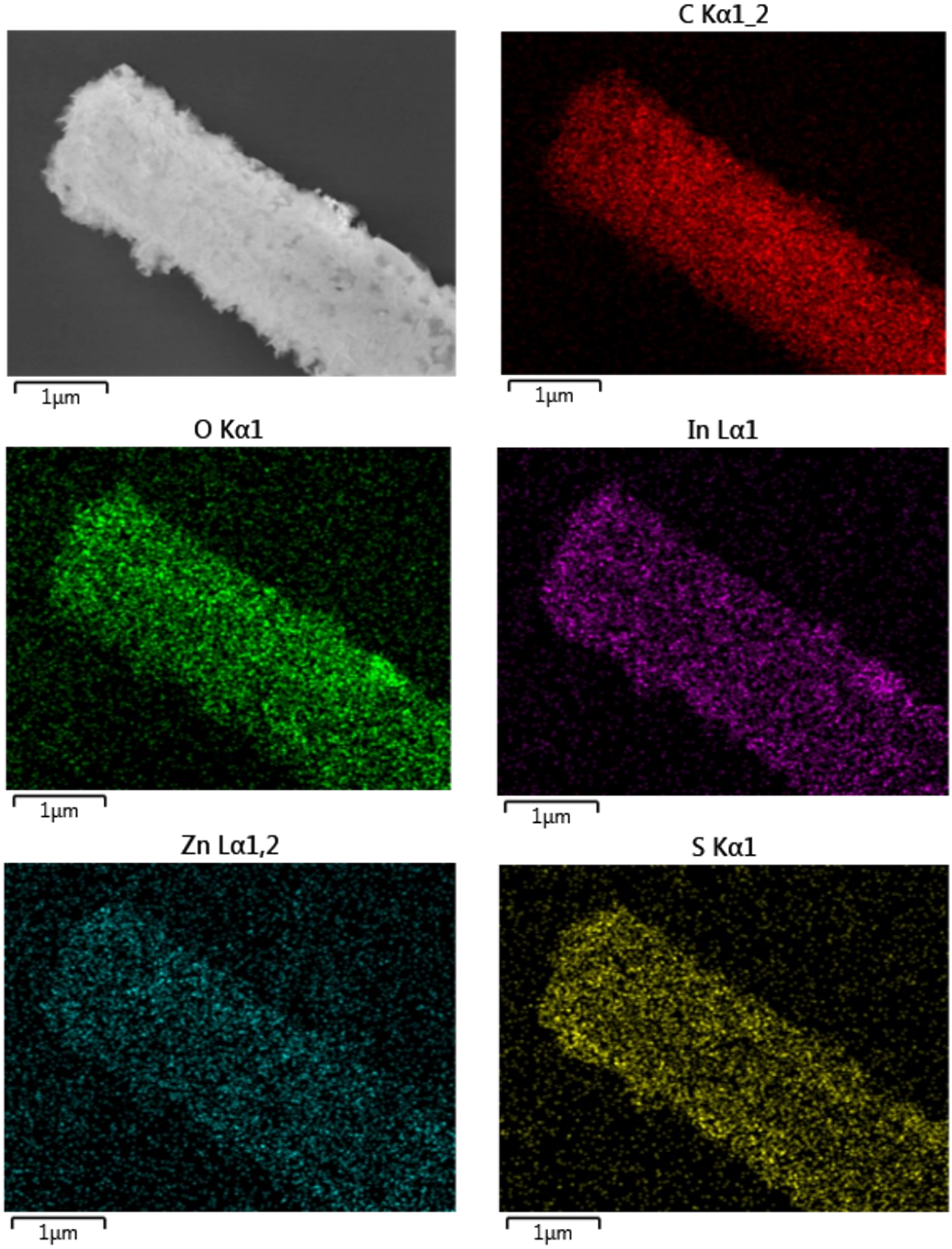

Figure S10. The corresponding STEM-EDX elemental mapping for

PCMT@In_2O_3/ZIS

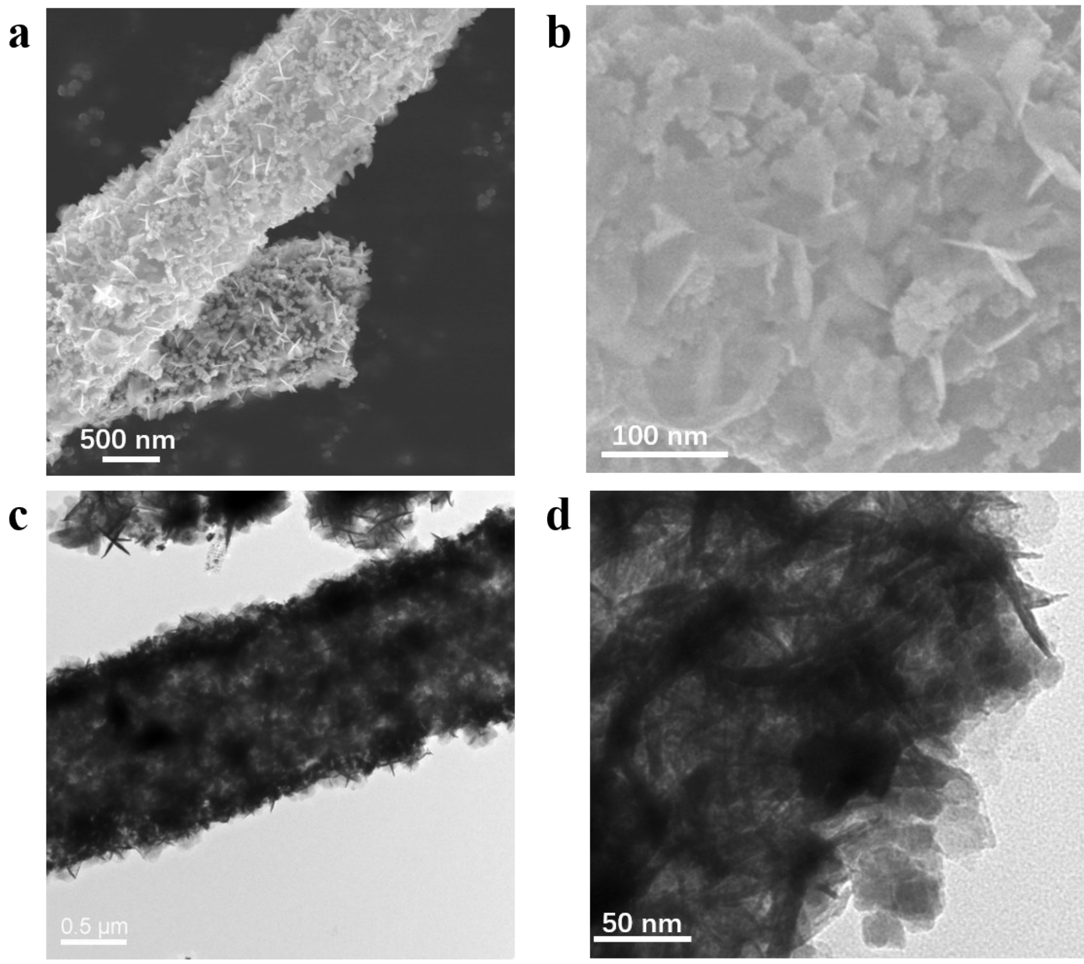

Figure S11. SEM and TEM images of PCMT@In_2O_3/ZIS after photocatalytic CO_2 conversion tests

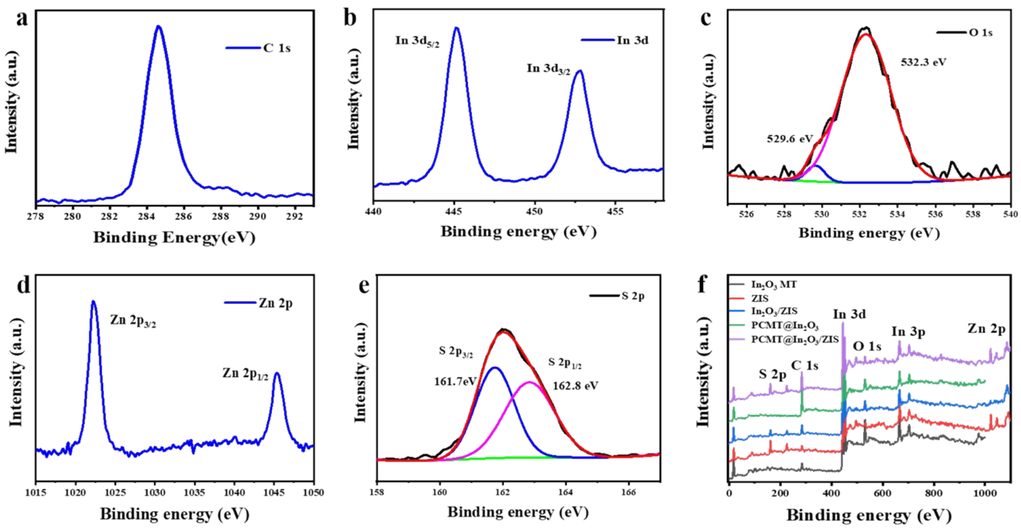

Figure S12. High-resolution spectra of (a) C 1s, (b) O 1s, (c) Zn 2p[3] (d) S 2p and (e) In 3d[5] of PCMT@In_2O_3/ZIS; (f) full XPS spectrum of different samples.

The In 3d high resolution XPS spectrum shows two peaks at 445.1 eV (In 3d $_{5/2}$) and 452.8 eV (In 3d $_{3/2}$), corresponding to In^{3+}. In the high resolution XPS spectrum of O 1s (Figure S12c), the two peaks centered at 529.6 and 532.3 eV are attributed to the oxygen in In-O-In ($O_{lattice}$) and the oxygen defects in metal oxide support (O_{defect}), respectively. The Zn 2p XPS spectrum splits into $2p_{3/2}$ (1022.2 eV) and 2p $_{1/2}$ (1045.2 eV) peaks, consistent with the values for Zn^{2+}. The S $2p_{3/2}$ peak at 161.7 eV is ascribed to S coordinated to Zn and In in $ZnIn_2S_4$. All the results indicate the chemical states of elements in PCMT@In_2O_3/ZIS heterostructures are In^{3+}, O^{2-}, Zn^{2+}, and S^{2-}.

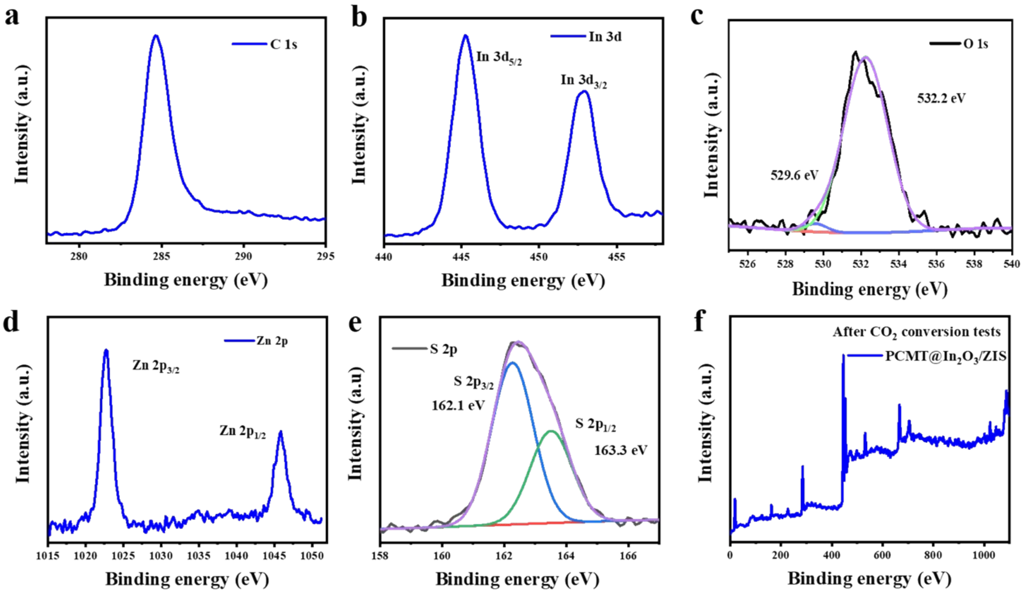

Figure S13. High-resolution spectra of (a) C 1s, (b) In $3d^5$, (c) O 1s, (d) Zn $2p^3$, (e) S 2p, and (f) full XPS spectrum of PCMT@In_2O_3/ZIS samples after photocatalytic CO_2 conversion tests.

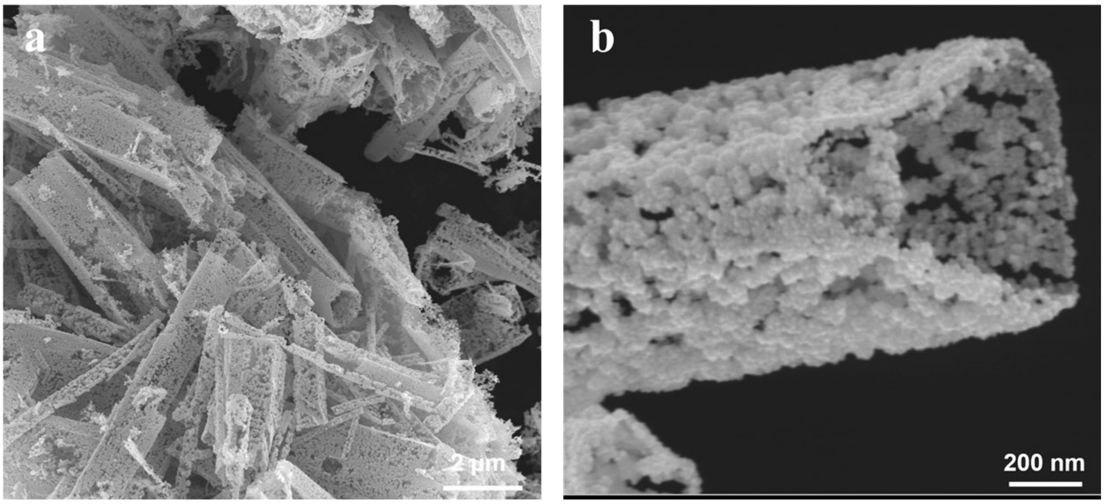

Figure S14. (a, b) SEM images of In_2O_3 MT with well-defined open ends after calcination.

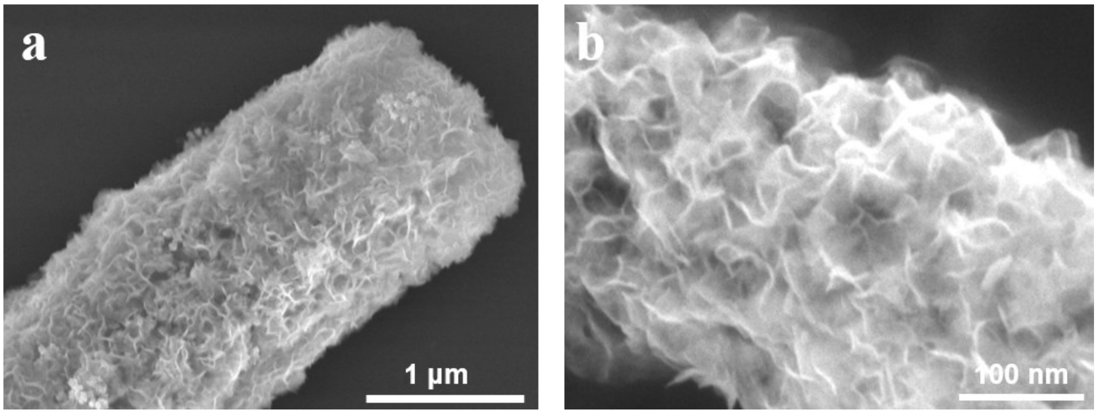

Figure S15. (a, b) SEM images of In_2O_3/ZIS.

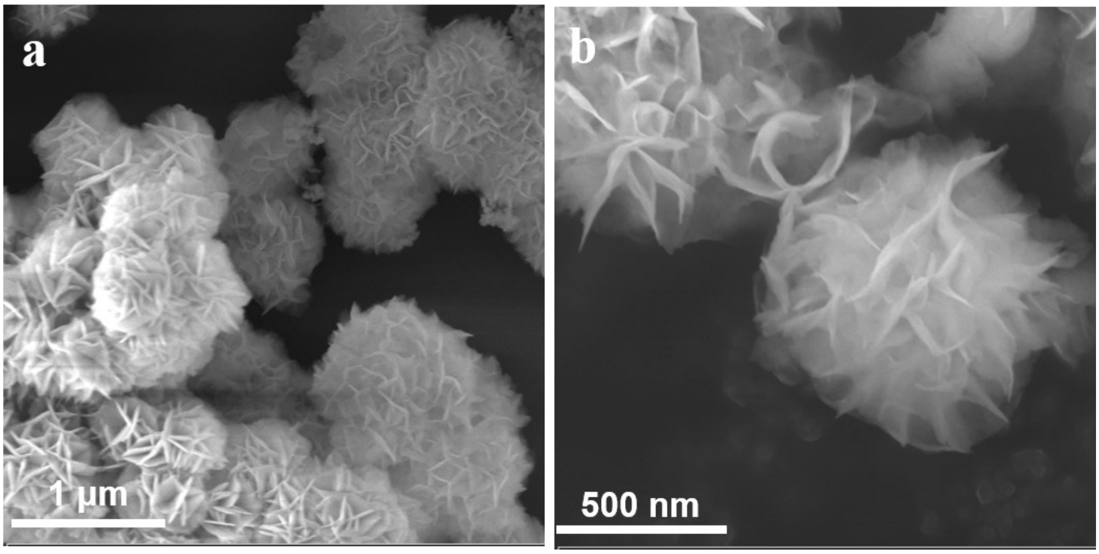

Figure S16. (a, b) FE-SEM images of ZIS nanosheets.

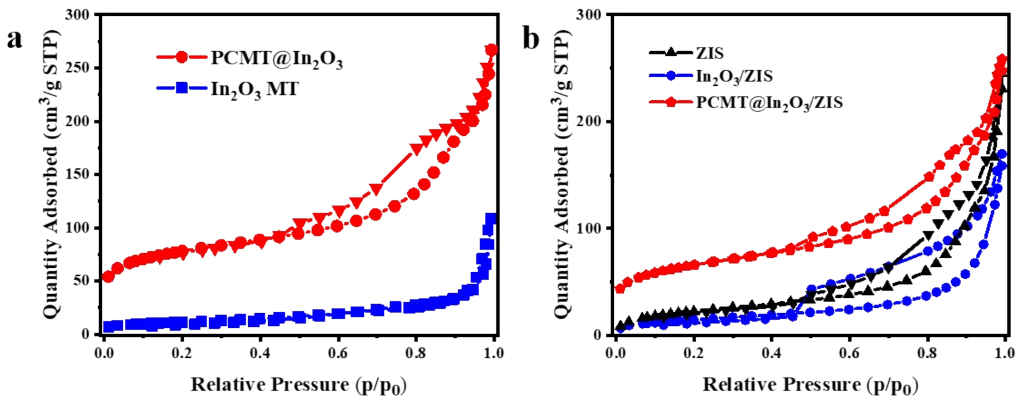

Figure S17. (a) Typical N_2 gas adsorption-desorption isotherm of In_2O_3 MT and PCMT@In_2O_3. (b) Typical N_2 gas adsorption-desorption isotherm of ZIS, In_2O_3/ZIS, and PCMT@In_2O_3/ZIS.

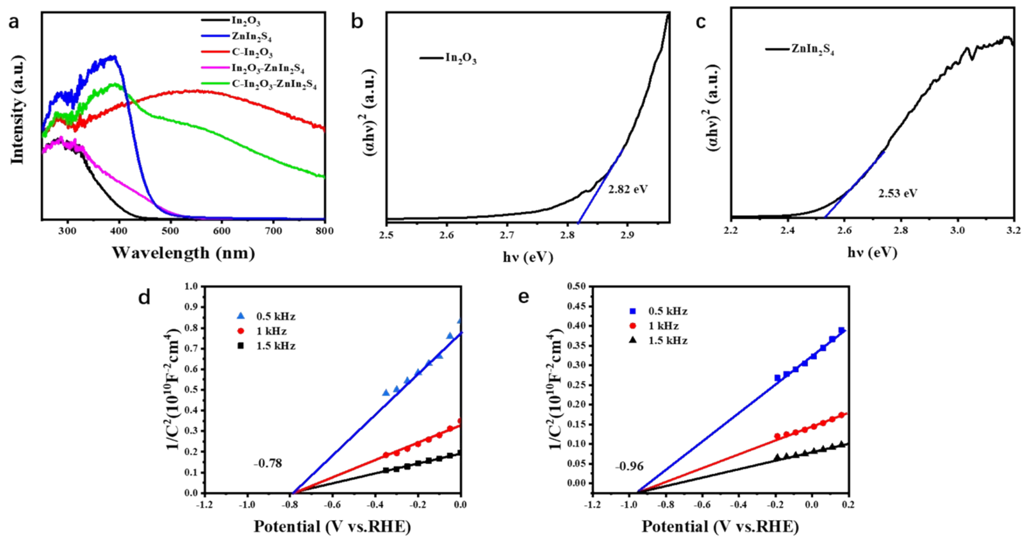

Figure S18. (a) UV−vis diffuse reflectance spectra of various photocatalysts; (b, c) Tauc plots of individual In_2O_3 and ZIS, and the bandgap energies are calculated 2.82 and 2.53 eV, respectively. (d, e) Mott−Schottky plots of individual In_2O_3 and ZIS.

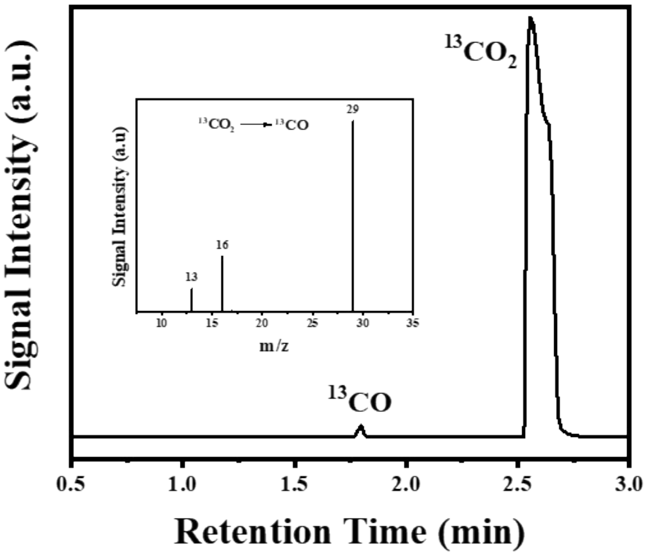

Figure S19. Gas chromatogram and mass spectra of ^{13}CO (inset) produced over PCMT@In_2O_3/ZIS. Carbon dioxide $^{13}CO_2$ was used.

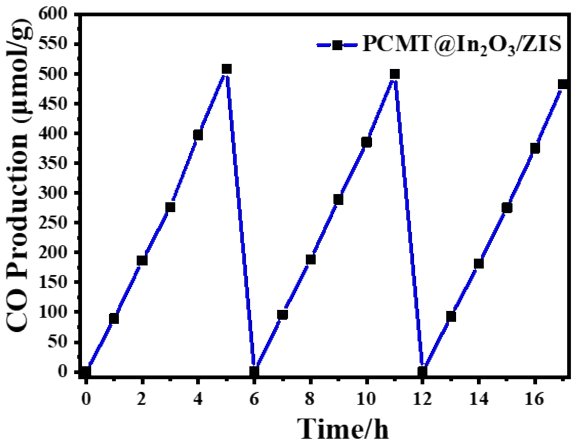

Figure S20. The cycle experiment test of PCMT@In_2O_3/ZIS.

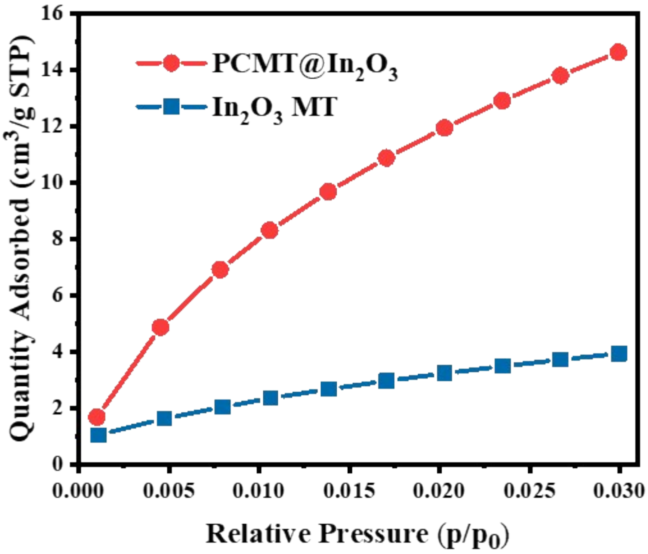

Figure S21. Typical CO_2 gas adsorption isotherm of In_2O_3 MT and PCMT@In_2O_3.

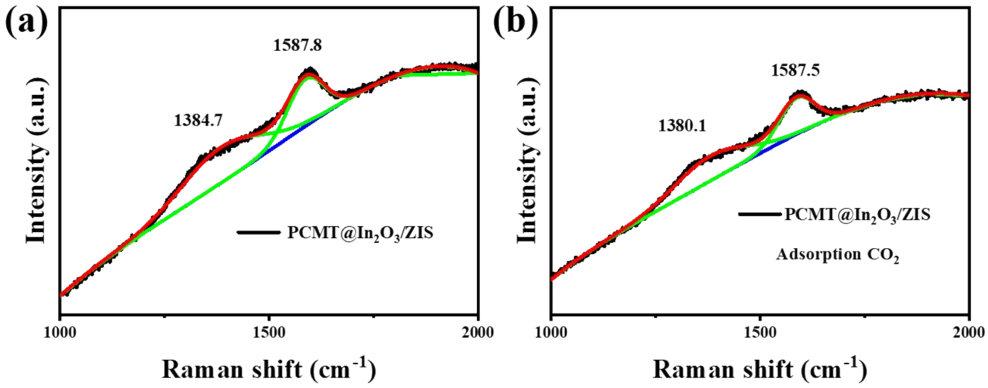

Figure S22. Raman spectroscopy of the PCMT@In_2O_3/ZIS (a) before and (b) after absorption CO_2.

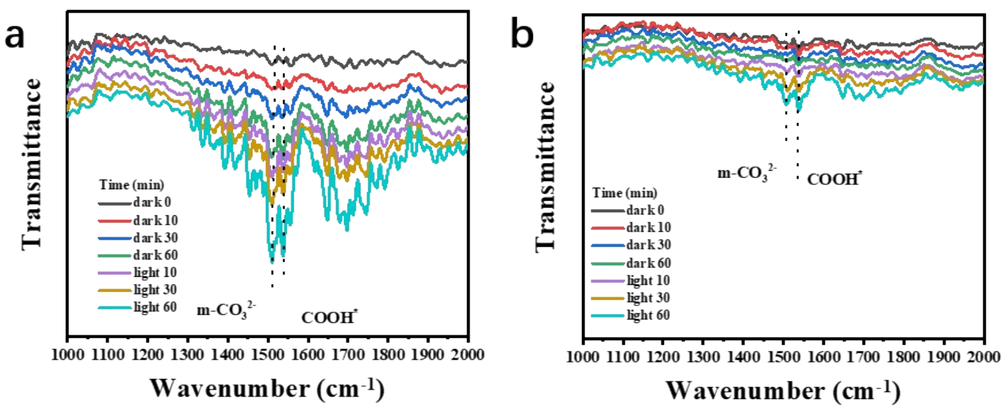

Figure S23. *In-situ* Fourier transformation infrared (FTIR) spectra of (a) PCMT@In_2O_3 and (b) In_2O_3 MT.

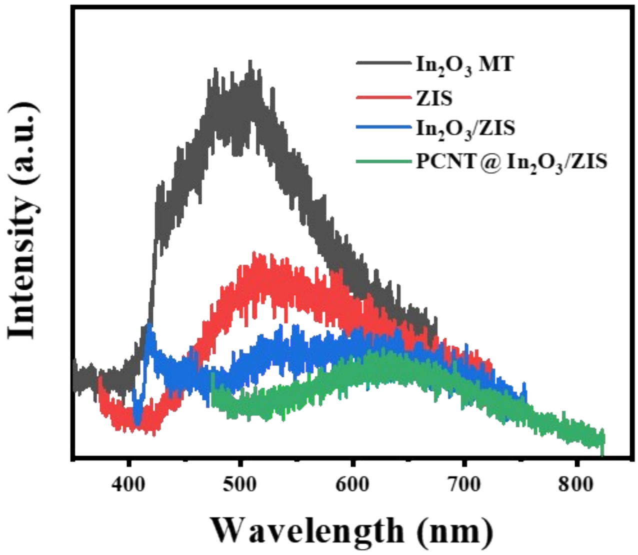

Figure S24. PL spectra of various materials.

Table S1. The photocatalytic CO_2 reduction performance of PCMT@In_2O_3/ZIS compared with other similar systems.

Catalyst	Light source	Cocatalyst	Sacrificial agent	Major product evolution rate (μmol h^{-1} g^{-1})	Ref.
PCMT@In_2O_3/IS	**300W Xenon lamp, 100mWcm^{-2}, AM1.5G**			**101.62**	**This work**
3D-ZIS	**300W Xenon lamp, 100mWcm^{-2}, AM1.5G**		**TEOA**	**CO: 276.6**	**[1]**
$ZnIn_2S_4$-In_2O_3	**300W Xe lamp with a 400 nm longpass cutoff filter**	**$Co(bpy)_3^{2+}$**	**TEOA**	**CO: 3075**	**[2]**
C-In_2O_3	**Xe-lamp (300 W)**	**Pt**		**CO: 633**	**[3]**
BCN	**300 W xenon lamp with 420 nm cutoff filter**	**$Co(bpy)_3^{2+}$**	**TEOA**	**CO: 94**	**[4]**
One-Unit-Cell $ZnIn_2S_4$	**300W Xenon lamp, 100mWcm^{-2}, AM1.5G**			**CO: 33.2**	**[5]**
TiO_2 nanotubes	**300W Xenon lamp, 100 mWcm^{-2}, AM1.5G**			**CO: 25 ppm**	**[6]**
HR-CN	**300 W Xe-lamp (λ>420 nm)**	**$Co(bpy)_3^{2+}$**	**TEOA**	**CO: 297**	**[7]**
In_2S_3−$CdIn_2S_4$	**300 W Xe-lamp $\lambda \geq$ 400 nm**	**$Co(bpy)_3^{2+}$**	**TEOA**	**CO: 825**	**[8]**
Ag-Cu_2O/ZnO NRs	**300 W Xe lamp, λ = 320-780 nm, 820 mW cm^{-2}**			**CO: 13.45**	**[9]**
ZnS-DETA/CdS	**300 W xenon lamp with 420 nm cutoff filter**	**$Co(bpy)_3^{2+}$**	**TEOA**	**CO: 33.3**	**[10]**

References

1 Y. He, H. Rao, K. Song, J. Li, Y. Yu, Y. Lou, C. Li, Y. Han, Z. Shi and S. Feng, *Adv. Funct. Mater.*, 2019, **29**, 1–10.

2 S. Wang, B. Y. Guan and X. W. D. Lou, *J. Am. Chem. Soc.*, 2018, 140, 5037–5040.

3 Y. X. Pan, Y. You, S. Xin, Y. Li, G. Fu, Z. Cui, Y. L. Men, F. F. Cao, S. H. Yu and J. B. Goodenough, *J. Am. Chem. Soc.*, 2017, **139**, 4123–4129.

4 C. Huang, C. Chen, M. Zhang, L. Lin, X. Ye, S. Lin, M. Antonietti and X. Wang, *Nat. Commun.*, DOI:10.1038/ncomms8698.

5 X. Jiao, Z. Chen, X. Li, Y. Sun, S. Gao, W. Yan, C. Wang, Q. Zhang, Y. Lin, Y. Luo and Y. Xie, *J. Am. Chem. Soc.*, 2017, **139**, 7586–7594.

6 X. Feng, J. D. Sloppy, T. J. Latempa, M. Paulose, S. Komarneni, N. Bao and C. A. Grimes, *J. Mater. Chem.*, 2011, **21**, 13429–13433.

7 Y. Zheng, L. Lin, X. Ye, F. Guo and X. Wang, *Angew. Chemie - Int. Ed.*, 2014, **53**, 11926–11930.

8 S. Wang, B. Y. Guan, Y. Lu and X. W. Lou, *J. Am. Chem. Soc.*, 2017, **139**, 17305–17308.

9 F. Zhang, Y. H. Li, M. Y. Qi, Z. R. Tang and Y. J. Xu, *Appl. Catal. B Environ.*, 2020, **268**, 118380.

10 B. Su, L. Huang, Z. Xiong, Y. Yang, Y. Hou, Z. Ding and S. Wang, *J. Mater. Chem. A*, 2019, **7**, 26877–26883.